

Spin crossover in the Prussian blue analogue  $\text{FePt}(\text{CN})_6$  induced  
by pressure or X-ray irradiation

SUPPLEMENTARY INFORMATION

Hanna L. B. Boström,<sup>a\*</sup> Andrew B. Cairns,<sup>b</sup> Lei Liu,<sup>c</sup> Peter Lazor,<sup>c</sup> and Ines E. Collings<sup>\*d</sup>

<sup>a</sup> Department of Chemistry, Uppsala Universitet, Ångströmlaboratoriet,  
Lägerhyddsvägen 1, 751 21 Uppsala, Sweden

<sup>b</sup> Department of Materials, Imperial College London, Royal School of Mines,  
Exhibition Road, SW7 2AZ, UK

<sup>c</sup> Department of Earth Sciences, Uppsala Universitet, Villavägen 16,  
752 36, Uppsala, Sweden

<sup>d</sup> Centre of X-ray Analytics, Swiss Federal Laboratories for Materials Science and Technology,  
Überlandstraße 129, 8600 Dübendorf, Switzerland

\*To whom correspondence should be addressed;

E-mail: hanna.bostrom@kemi.uu.se, ines.collings@empa.ch

# Contents

<b>1</b>	<b>Experimental details</b>	<b>3</b>
	Synthesis . . . . .	3
	Magnetometry . . . . .	3
	X-ray diffraction . . . . .	3
	Raman spectroscopy . . . . .	4
<b>2</b>	<b>Magnetometry</b>	<b>6</b>
<b>3</b>	<b>Variable-pressure X-ray diffraction</b>	<b>7</b>
<b>4</b>	<b>Raman spectroscopy</b>	<b>22</b>
<b>5</b>	<b>References</b>	<b>23</b>

# 1 Experimental details

## Synthesis

$\text{FePt}(\text{CN})_6$  was synthesised by the dropwise addition of  $\text{FeSO}_4$  (0.36 mmol, 0.5 ml) to a stoichiometric solution of  $\text{K}_2\text{Pt}(\text{CN})_6$  in 0.5 ml of  $\text{H}_2\text{O}$ . The reaction was stirred at ambient temperature for 1.5 h and the product was isolated as a white powder by filtration. The as-synthesised powder was dehydrated at  $80^\circ\text{C}$  under vacuum for 24 h prior to the high-pressure diffraction experiments.

## Magnetometry

Temperature-dependent magnetisation was measured using a Quantum Design MPMS SQUID magnetometer. The field-cooled magnetic moment was collected in the temperature range 10–300 K at  $H = 5000$  Oe with a step size of 1 K and a cooling rate of  $2\text{ K min}^{-1}$ .

## X-ray diffraction

The variable-pressure X-ray diffraction with Daphne oil as the pressure-transmitting medium (PTM) was performed on the I15 beamline at Diamond Light Source, UK, using a monochromatic X-ray beam with a wavelength of  $\lambda = 0.424112\text{ \AA}$ . The dehydrated  $\text{FePt}(\text{CN})_6$  sample was loaded into a membrane-driven diamond anvil cell (DAC), equipped with culets of  $400\text{ }\mu\text{m}$  diameter. Stainless steel was used as the gasket with a  $300\text{ }\mu\text{m}$  diameter sample hole. Daphne 7373 oil was employed as the PTM, and ruby spheres were added to the sample chamber for pressure calibration. The sample was loaded inside a glovebox in order to minimise re-hydration.

$\text{LaB}_6$  was employed as a calibrant prior to the measurements. The 2D diffraction images were collected using the PerkinElmer area detector, and the images were integrated using Dioptas.<sup>S1</sup> Aluminium plates were placed in front of the beam during DAC alignment in order to attenuate the beam when not measuring diffraction. For the powder measurements, the DAC was rotated by  $\pm 6^\circ$  during a continuous measurement with a duration of 30 s or 60 s.

The variable-pressure X-ray diffraction with MeOH as the PTM was performed on the P02.2 beamline at PETRA III, in Hamburg, Germany, using a monochromatic X-ray beam with a wavelength of  $\lambda = 0.2897\text{ \AA}$ . The beam size used was  $8.5 \times 3\text{ }\mu\text{m}$ . The dehydrated  $\text{FePt}(\text{CN})_6$  sample was loaded into a membrane-driven diamond anvil cell, equipped with culets of  $400\text{ }\mu\text{m}$

diameter. Stainless steel was used as the gasket. MeOH was employed as the PTM, and ruby spheres were added to the sample chamber for pressure calibration. In this case, the loading was performed in air.

CeO<sub>2</sub> was employed as a calibrant prior to the measurements. The 2D diffraction images were collected using the PerkinElmer area detector, and the images were integrated using Dioptas.<sup>S1</sup> Platinum foil was placed in front of the beam during DAC alignment in order to attenuate the beam when not measuring diffraction. For the powder measurements, the DAC was rotated by  $\pm 3^\circ$  during a continuous measurement with a duration of 6 s. In the case of the long X-ray irradiation measurement at 0.6 GPa, the DAC was rotated to  $-28^\circ$ , and single frame collections with a measurement time of 4 s each were taken every  $0.5^\circ$  up to the DAC rotation angle of  $+28^\circ$ , giving a total of 112 frames. The pressure was measured before and after each measurement, and the average was taken.

Data analysis was carried out by Rietveld and Pawley refinements as implemented in the software TOPAS.<sup>S2-4</sup> The peakshape was modelled by a pseudo-Voigt function and the background by a Chebyshev polynomial. The data collected as a function of X-ray exposure were refined by sequential Rietveld refinements. To prevent divergence, the lattice parameters of the LS and HS phases were constrained to lie in the range of 10.18–10.23 Å and  $>10.45$  Å, respectively.

The variable-pressure unit cell lattice parameters were fitted using the second-order Birch–Murnaghan equation of state as implemented in the software EoSfit-GUI.<sup>S5-7</sup> Only data collected on compression were used. Inspection of the normalised pressure *vs.* Eulerian strain ( $f-F$ ) plots for all phases indicate a second-order fit is sufficient to account for the experimental  $p(V)$  data. Due to the initial pressure that had to be applied to ensure the DAC was closed with MeOH, no data could be measured in the very low pressure region (0–0.4(1) GPa). This results in a lack of restraint in the fitting of the  $p(V)$  data, in particular the value of the zero pressure volume. Therefore  $V_0$  was fixed to the experimentally determined value from our previous experiment (that is itself within error of the value refined from the B-M fit of that dataset), and  $B_0$  was refined.

## Raman spectroscopy

A pair of low-fluorescence diamond anvils with a culet size of 300  $\mu\text{m}$  was mounted on the symmetric cell designed to generate high pressures. A T301 stainless steel disk with an initial

thickness of 250  $\mu\text{m}$  was indented to around 30  $\mu\text{m}$  and used as a gasket. The diameter of the sample chamber drilled in the centre of the pre-indented gasket was around 100  $\mu\text{m}$ . Powdered sample, along with tiny ruby balls serving as a pressure gauge,<sup>S8</sup> and silicone oil as a pressure-transmitting medium were loaded into the sample chamber.

The high-pressure Raman spectra of  $\text{FePt}(\text{CN})_6$  were collected in the backscattering geometry using a green laser (532.42 nm) as the excitation source. The laser beam spot size was 2–4  $\mu\text{m}$  on the sample after focusing by a 20 X long working distance objective. Two holographic notch filters were used to reduce the Rayleigh peak intensity. The scattered light was analysed using the high-throughput single-stage imaging spectrometer (HoloSpec f/1.8i, Kaiser Optical Systems, Inc.) and collected by the CCD detector (Newton, Andor technology,  $1600 \times 400$  pixels, thermoelectrically cooled to  $-55^\circ\text{C}$ ). The system was calibrated using the fluorescence of neon lamp and the first-order Raman line of single-crystal silicon. Raman spectra were collected in the range 50–3100  $\text{cm}^{-1}$  at room temperature. The laser power was set to 2 mW in order to avoid sample heating or degeneration. The acquisition time of 10 s with 12 accumulations was employed to get a good signal-to-noise ratio. Peak positions were extracted by fitting a Lorentzian curve to the absorption lines.

## 2 Magnetometry

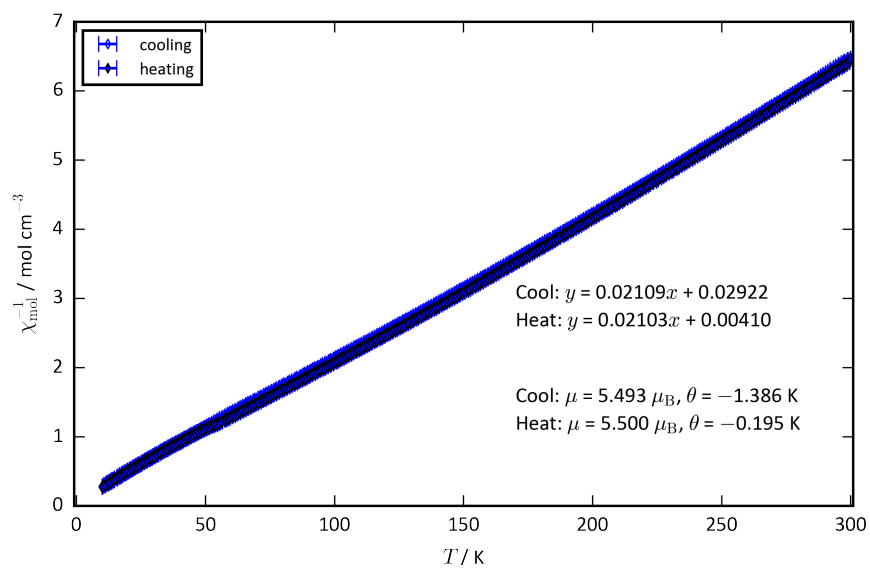


**Figure S1:** Curie-Weiss plot of  $\text{FePt}(\text{CN})_6$  with the equation for the line of best fit and the values for the effective magnetic moment ( $\mu$ ) and the Weiss constant ( $\Theta$ ) indicated.

### 3 Variable-pressure X-ray diffraction

**Table S1:** Lattice parameters as a function of pressure using Daphne oil as a PTM. Patterns collected at the same pressure point originate from different sample positions. Asterisks denote data collected on decompression. The uncertainty is  $\pm 0.1$  GPa for all pressure points.<sup>S9</sup>

$p$ / GPa	$a_{\text{HS}}$ / Å	HS phase fraction (%)	$a_{\text{LS}}$ / Å	LS phase fraction (%)
0.0	10.60767(5)	100		
0.14	10.59589(5)	100		
0.22	10.58649(6)	100		
0.37	10.56847(6)	100		
0.71	10.53393(7)	100		
0.83	10.5169(5)	37.2(2)	10.2008(3)	62.8(2)
0.83	10.5258(2)	80.63(15)	10.1989(6)	19.37(15)
0.83	10.5209(4)	47.7(2)	10.2001(4)	52.3(2)
0.92			10.19332(12)	100
1.03			10.17845(10)	100
1.03			10.18019(10)	100
1.20			10.15976(8)	100
1.35			10.14421(7)	100
1.59			10.12204(7)	100
1.78			10.10255(9)	100
2.00			10.08488(14)	100
2.00			10.0841(2)	100
2.23			10.0699(2)	100
2.23			10.0692(3)	100
2.48			10.0568(3)	100
2.48			10.0559(3)	100
2.81			10.0465(4)	100
2.99			10.0410(5)	100
2.99			10.0412(6)	100

Continued on next page

Table S1 – continued from previous page

$p$ / GPa	$a_{\text{HS}}$ / Å	HS phase fraction (%)	$a_{\text{LS}}$ / Å	LS phase fraction (%)
2.00*			10.0825(3)	100
1.06*			10.15794(10)	100
0.90*			10.17374(11)	100
0.84*			10.17891(11)	100
0.79*			10.1892(2)	100
0.71*			10.1960(3)	100
0.66*			10.2079(9)	100
0.60*	10.5115(3)	100		
0.51*	10.52137(14)	100		
0.02*	10.59017(6)	100		
0.02*	10.60343(6)	100		

**Table S2:** Lattice parameters as a function of pressure using MeOH as a PTM. The uncertainty is  $\pm 0.1$  GPa for all pressure points.<sup>S9</sup>

$p$ / GPa	$a_{\text{HS}}$ / Å	HS phase fraction (%)	$a_{\text{LS}}$ / Å	LS phase fraction (%)
0.44	10.5647(6)	100		
0.59	10.5642(6)	100		
0.66	10.5261(11)	100		
0.73	10.5359(7)	100		
0.93	10.493(3)	12.8(4)	10.1690(10)	87.2(4)
0.93	10.497(2)	26.6(4)	10.1704(13)	73.4(4)
0.93	10.4982(15)	22.7(3)	10.1698(9)	77.3(3)
1.07			10.1605(7)	100
1.18			10.1580(9)	100
1.43			10.1374(10)	100
1.43			10.1416(8)	100
1.79			10.1140(11)	100
1.79			10.1136(7)	100
2.06			10.1015(6)	100
2.62			10.0722(8)	100
3.18			10.0493(10)	100

**Table S3:** Lattice parameters and phase fractions as a function of X-ray exposure at 0.6 GPa.

run no	$a_{\text{HS}} / \text{\AA}$	HS phase fraction (%)	$a_{\text{LS}} / \text{\AA}$	LS phase fraction (%)
1	10.5489(11)	99.7(13)		
2	10.5391(6)	100.0(6)		
3	10.5307(10)	100.0(11)		
4	10.5168(6)	99.9(7)		
5	10.5122(5)	100.0(6)		
6	10.5033(7)	100.0(7)		
7	10.4986(9)	100.0(8)		
8	10.4892(9)	94.7(8)	10.227(15)	5.3(8)
9	10.4877(8)	84.7(6)	10.230(5)	15.3(6)
10	10.4877(8)	87.8(6)	10.230(6)	12.2(6)
11	10.4911(9)	85.3(6)	10.230(5)	14.7(6)
12	10.4910(8)	82.6(6)	10.230(4)	17.4(6)
13	10.4940(10)	90.0(8)	10.219(8)	10.0(8)
14	10.4917(9)	88.3(7)	10.229(6)	11.7(7)
15	10.4934(9)	89.3(7)	10.230(7)	10.7(7)
16	10.4873(10)	84.7(7)	10.230(5)	15.3(7)
17	10.4743(10)	75.8(7)	10.230(4)	24.2(7)
18	10.4778(9)	77.3(6)	10.230(3)	22.7(6)
19	10.4745(9)	77.9(6)	10.230(3)	22.1(6)
20	10.4733(9)	73.8(6)	10.230(3)	26.2(6)
21	10.4681(10)	65.8(7)	10.230(2)	34.2(7)
22	10.4622(11)	63.3(7)	10.230(2)	36.7(7)
23	10.4636(11)	66.2(7)	10.230(2)	33.8(7)
24	10.4612(12)	61.7(7)	10.230(2)	38.3(7)
25	10.4552(14)	47.2(7)	10.2300(12)	52.8(7)
26	10.457(2)	42.3(8)	10.2283(12)	57.7(8)
27	10.4625(12)	46.6(6)	10.2296(11)	53.4(6)

Continued on next page

Table S3 – continued from previous page

run no	$a_{\text{HS}} / \text{\AA}$	HS phase fraction (%)	$a_{\text{LS}} / \text{\AA}$	LS phase fraction (%)
28	10.4694(14)	54.6(8)	10.230(2)	45.4(8)
29	10.473(2)	49.2(9)	10.227(2)	50.8(9)
30	10.4675(14)	44.9(7)	10.2260(12)	55.1(7)
31	10.470(2)	35.1(6)	10.2226(8)	64.9(6)
32	10.469(2)	32.7(6)	10.2248(8)	67.3(6)
33	10.4740(14)	33.6(5)	10.2242(7)	66.4(5)
34	10.464(3)	28.9(7)	10.2169(9)	71.1(7)
35	10.461(2)	28.2(6)	10.2178(8)	71.8(6)
36	10.464(2)	28.0(6)	10.2176(7)	72.0(6)
37	10.468(3)	26.2(6)	10.2147(8)	73.8(6)
38	10.460(3)	27.5(7)	10.2147(9)	72.5(7)
39	10.459(3)	25.9(7)	10.2147(9)	74.1(7)
40	10.453(2)	28.8(6)	10.2166(8)	71.2(6)
41	10.448(3)	27.5(7)	10.2166(9)	72.5(7)
42	10.456(3)	24.9(6)	10.2149(8)	75.1(6)
43	10.452(4)	22.2(8)	10.2109(10)	77.8(8)
44	10.455(2)	28.9(5)	10.2140(7)	71.1(5)
45	10.449(3)	28.6(7)	10.2164(9)	71.4(7)
46	10.457(3)	26.6(6)	10.2137(8)	73.4(6)
47	10.468(2)	35.0(6)	10.2149(9)	65.0(6)
48	10.474(3)	32.8(7)	10.2117(10)	67.2(7)
49	10.4782(14)	33.9(5)	10.2096(7)	66.1(5)
50	10.4779(13)	41.3(6)	10.2162(9)	58.7(6)
51	10.4786(14)	42.3(6)	10.2217(10)	57.7(6)
52	10.4792(15)	38.0(6)	10.2205(9)	62.0(6)
53	10.463(2)	32.2(6)	10.2160(9)	67.8(6)
54	10.460(4)	26.6(8)	10.2120(12)	73.4(8)
55	10.462(3)	26.1(7)	10.2123(9)	73.9(7)

Continued on next page

Table S3 – continued from previous page

run no	$a_{\text{HS}} / \text{\AA}$	HS phase fraction (%)	$a_{\text{LS}} / \text{\AA}$	LS phase fraction (%)
56	10.465(2)	27.6(5)	10.2141(7)	72.4(5)
57	10.465(2)	27.8(5)	10.2148(6)	72.2(5)
58	10.4668(14)	32.3(5)	10.2142(7)	67.7(5)
59	10.4648(15)	30.1(5)	10.2153(7)	69.9(5)
60	10.464(2)	27.0(5)	10.2149(7)	73.0(5)
61	10.4657(14)	26.3(4)	10.2162(5)	73.7(4)
62	10.463(2)	27.1(5)	10.2167(6)	72.9(5)
63	10.460(3)	22.0(5)	10.2137(7)	78.0(5)
64	10.468(3)	22.0(5)	10.2129(6)	78.0(5)
65	10.474(2)	21.7(4)	10.2124(5)	78.3(4)
66	10.473(3)	20.8(5)	10.2129(6)	79.2(5)
67	10.471(3)	18.0(5)	10.2120(6)	82.0(5)
68	10.474(4)	17.4(6)	10.2114(7)	82.6(6)
69	10.464(3)	17.8(6)	10.2119(7)	82.2(6)
70	10.458(3)	18.1(5)	10.2123(6)	81.9(5)
71	10.463(3)	18.4(4)	10.2130(5)	81.6(4)
72	10.460(3)	18.6(5)	10.2130(6)	81.4(5)
73	10.466(3)	19.8(5)	10.2147(7)	80.2(5)
74	10.465(3)	19.5(5)	10.2174(6)	80.5(5)
75	10.471(3)	19.9(5)	10.2182(6)	80.1(5)
76	10.468(3)	19.8(5)	10.2171(6)	80.2(5)
77	10.454(3)	19.6(5)	10.2179(6)	80.4(5)
78	10.441(3)	18.2(5)	10.2155(6)	81.8(5)
79	10.439(4)	17.7(6)	10.2157(8)	82.3(6)
80	10.436(4)	19.1(7)	10.2160(8)	80.9(7)
81	10.437(4)	19.3(7)	10.2145(8)	80.7(7)
82	10.445(3)	24.1(5)	10.2159(7)	75.9(5)
83	10.449(3)	18.1(5)	10.2162(6)	81.9(5)

Continued on next page

Table S3 – continued from previous page

run no	$a_{\text{HS}} / \text{\AA}$	HS phase fraction (%)	$a_{\text{LS}} / \text{\AA}$	LS phase fraction (%)
84	10.445(4)	16.2(6)	10.2160(7)	83.8(6)
85	10.459(4)	13.7(5)	10.2164(6)	86.3(5)
86	10.470(4)	15.9(6)	10.2183(7)	84.1(6)
87	10.477(5)	15.0(6)	10.2180(8)	85.0(6)
88	10.473(4)	17.7(6)	10.2173(8)	82.3(6)
89	10.477(4)	18.9(6)	10.2158(8)	81.1(6)
90	10.478(3)	18.2(5)	10.2161(6)	81.8(5)
91	10.457(4)	16.6(5)	10.2143(7)	83.4(5)
92	10.455(3)	17.0(5)	10.2157(6)	83.0(5)
93	10.464(3)	17.9(5)	10.2165(7)	82.1(5)
94	10.468(3)	19.9(5)	10.2169(6)	80.1(5)
95	10.461(3)	16.5(5)	10.2173(6)	83.5(5)
96	10.468(3)	17.1(5)	10.2165(6)	82.9(5)
97	10.457(4)	17.3(5)	10.2152(7)	82.7(5)
98	10.452(4)	15.8(5)	10.2183(7)	84.2(5)
99	10.459(5)	13.9(6)	10.2168(7)	86.1(6)
100	10.443(5)	12.8(6)	10.2145(7)	87.2(6)
101	10.432(6)	13.0(7)	10.2125(8)	87.0(7)
102	10.430(7)	12.4(8)	10.2118(9)	87.6(8)
103	10.430(7)	13.7(9)	10.2127(11)	86.3(9)
104	10.430(5)	14.7(7)	10.2146(8)	85.3(7)
105	10.430(5)	14.6(7)	10.2163(9)	85.4(7)
106	10.438(7)	12.9(8)	10.2179(9)	87.1(8)
107	10.440(7)	11.9(8)	10.2165(9)	88.1(8)
108	10.444(6)	12.7(7)	10.2151(8)	87.3(7)
109	10.440(6)	12.4(7)	10.2159(8)	87.6(7)
110	10.442(6)	13.9(8)	10.2174(9)	86.1(8)
111	10.432(6)	16.0(9)	10.2183(11)	84.0(9)

Continued on next page

**Table S3 – continued from previous page**

run no	$a_{\text{HS}} / \text{\AA}$	HS phase fraction (%)	$a_{\text{LS}} / \text{\AA}$	LS phase fraction (%)
112	10.436(6)	16.6(9)	10.2220(12)	83.4(9)

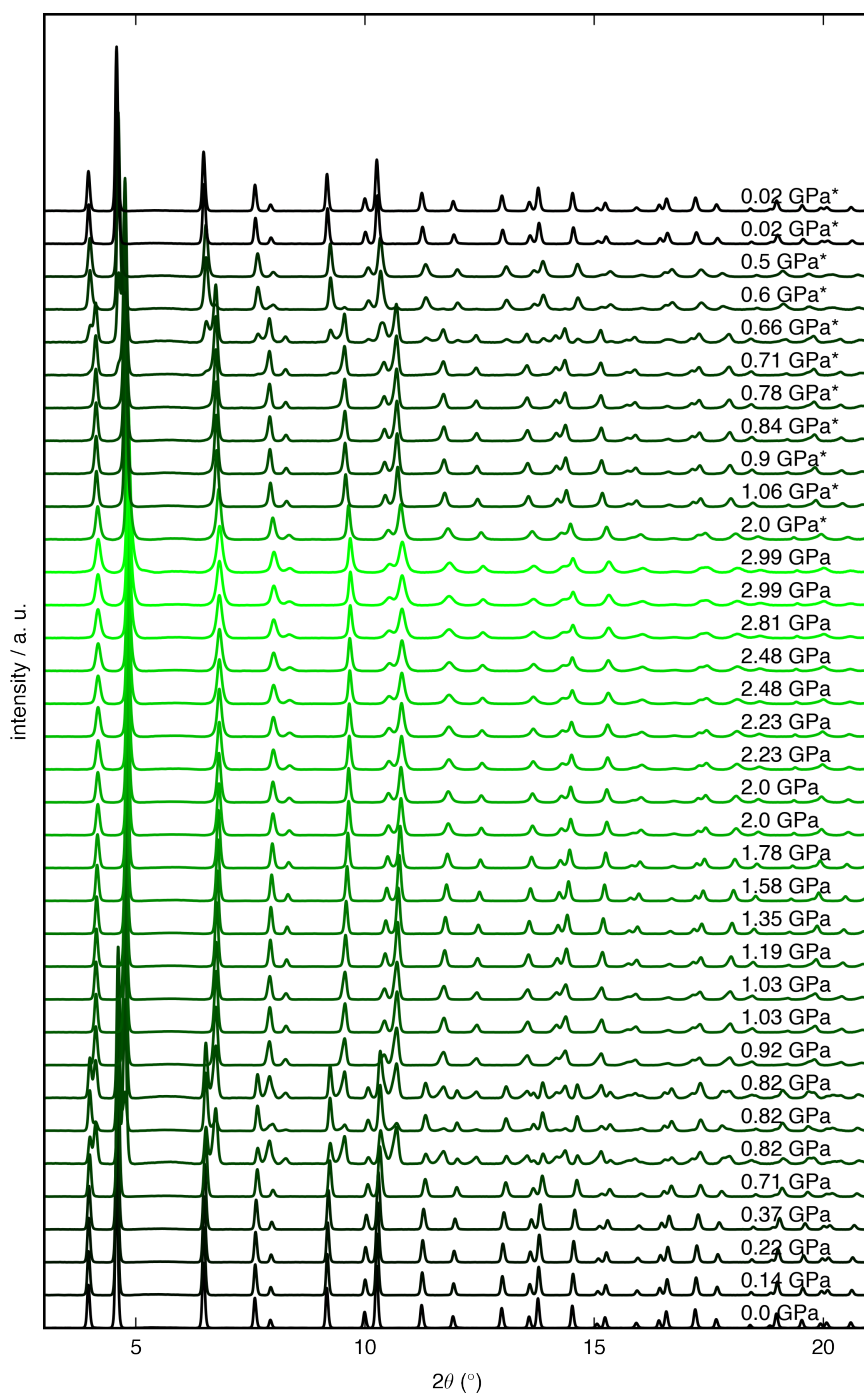


**Figure S2:** The XRD patterns of  $\text{FePt}(\text{CN})_6$  as a function of pressure using Daphne oil as a PTM with  $\lambda = 0.424112 \text{ \AA}$ . Data were collected on compression and patterns collected on decompression are indicated by an asterisk. Patterns collected at the same pressure point originate from different sample positions. The intensity variations of these patterns are attributed to their different radiation history.

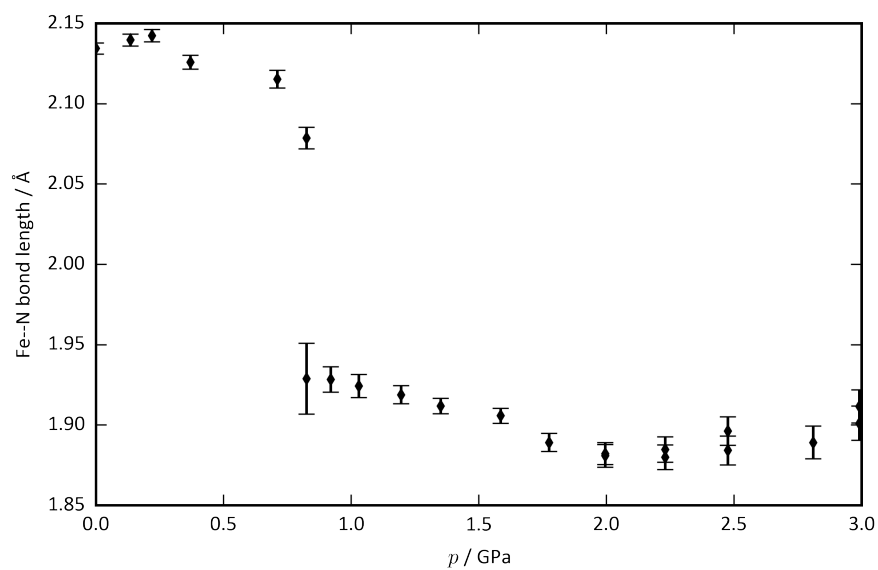


**Figure S3:** The Fe–N bond length as a function of pressure using Daphne oil as a PTM.

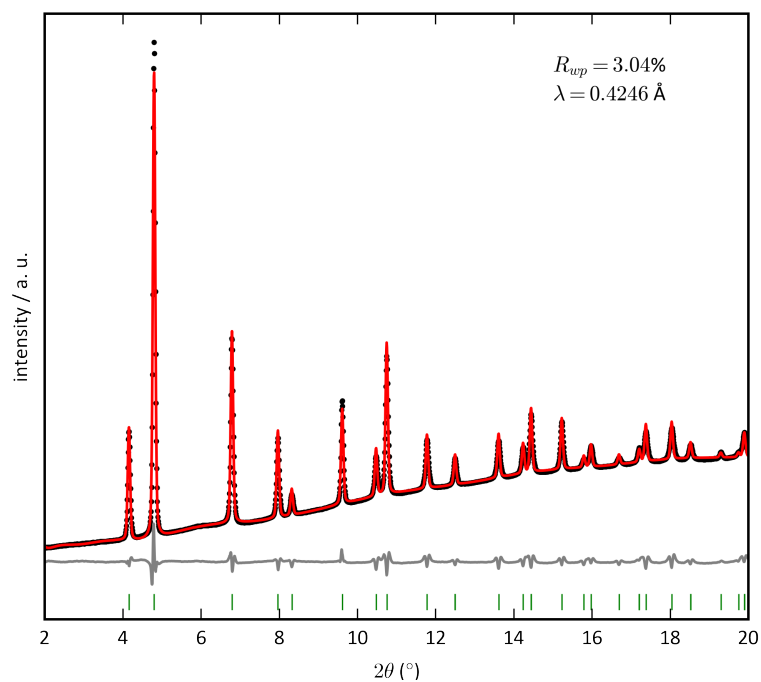


**Figure S4:** The Rietveld refinement of LS Phase of  $\text{FePt}(\text{CN})_6$  at 1.59 GPa using Daphne oil as a PTM. The data is shown in black, the simulated data in red, allowed reflections by green vertical bars and the difference curve in grey.

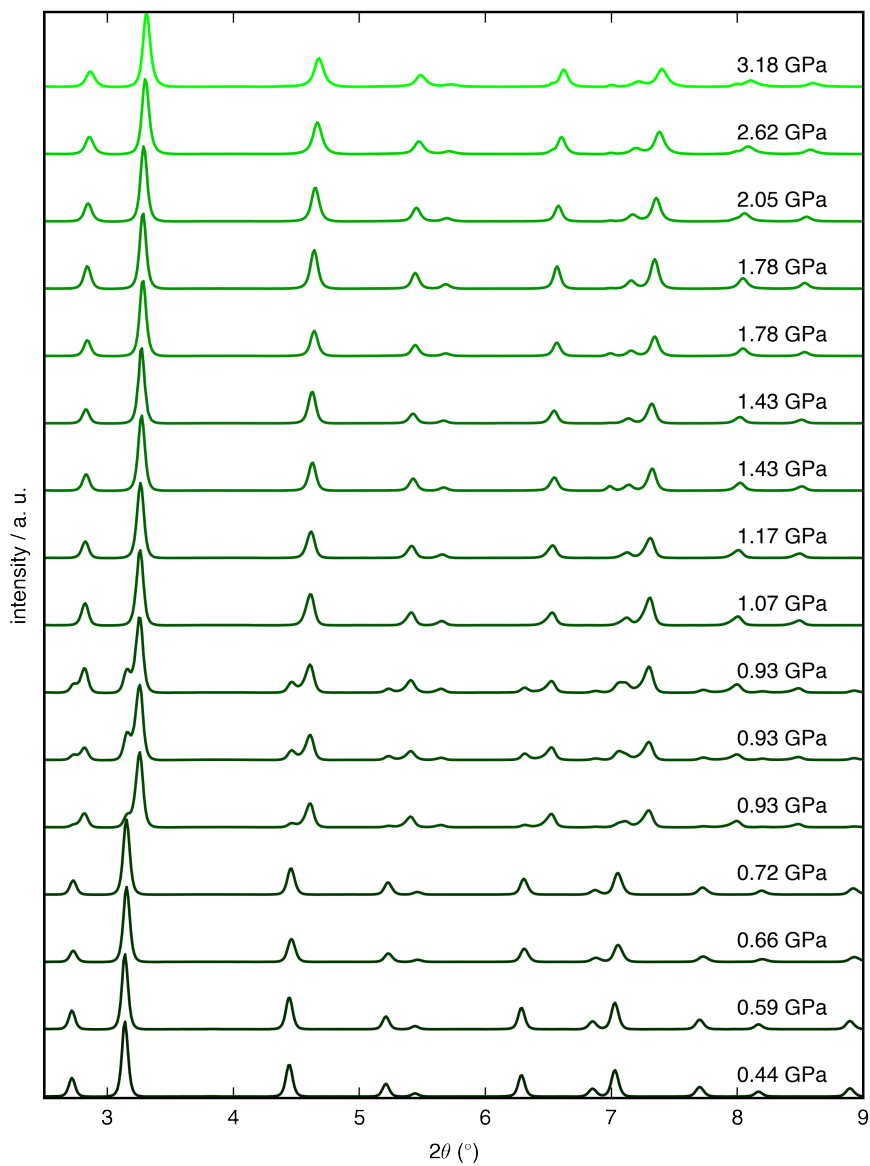


**Figure S5:** The XRD patterns of FePt(CN)<sub>6</sub> as a function of pressure using MeOH as a pressure-transmitting medium with  $\lambda = 0.2897 \text{ \AA}$ . Patterns collected at the same pressure point originate from different sample positions.

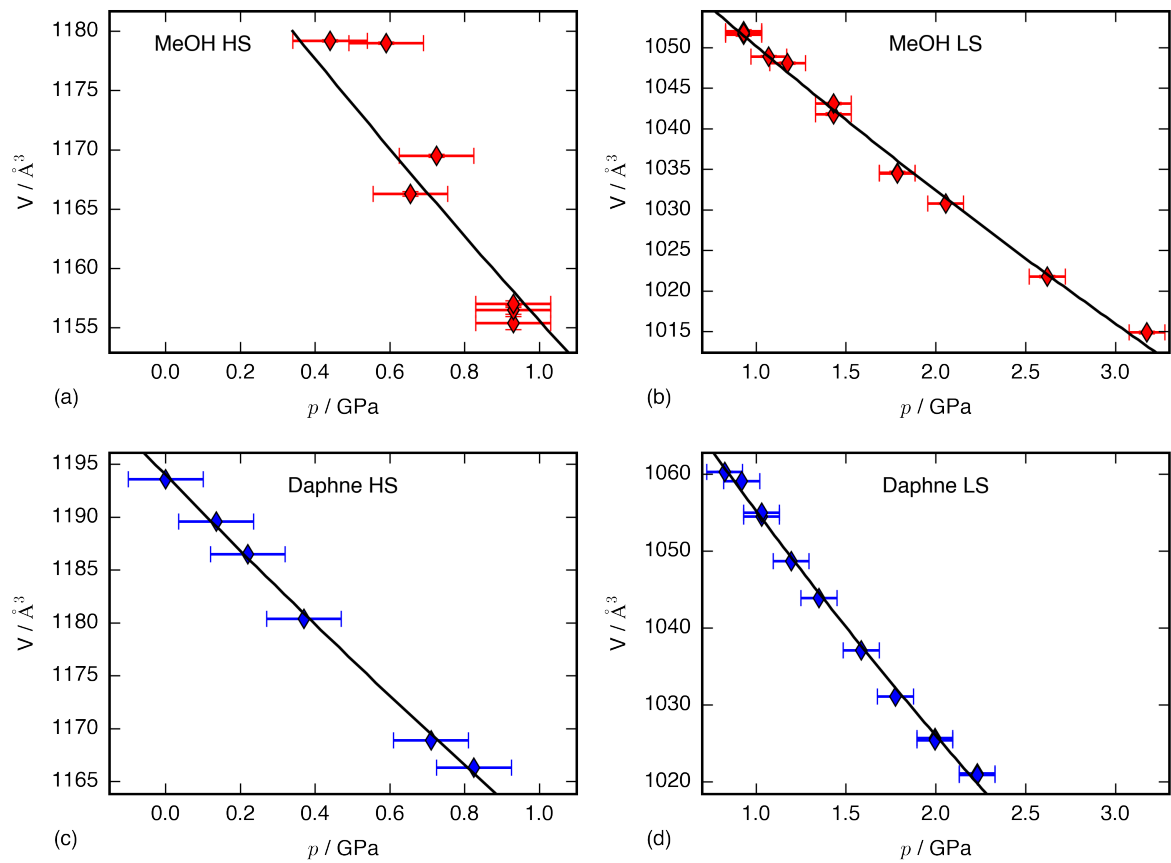


**Figure S6:** The second-order Birch–Murnaghan fits of the volume for the (a) HS phase in MeOH, (b) LS phase in MeOH, (c) HS phase in Daphne oil, and (d) LS phase in Daphne oil.

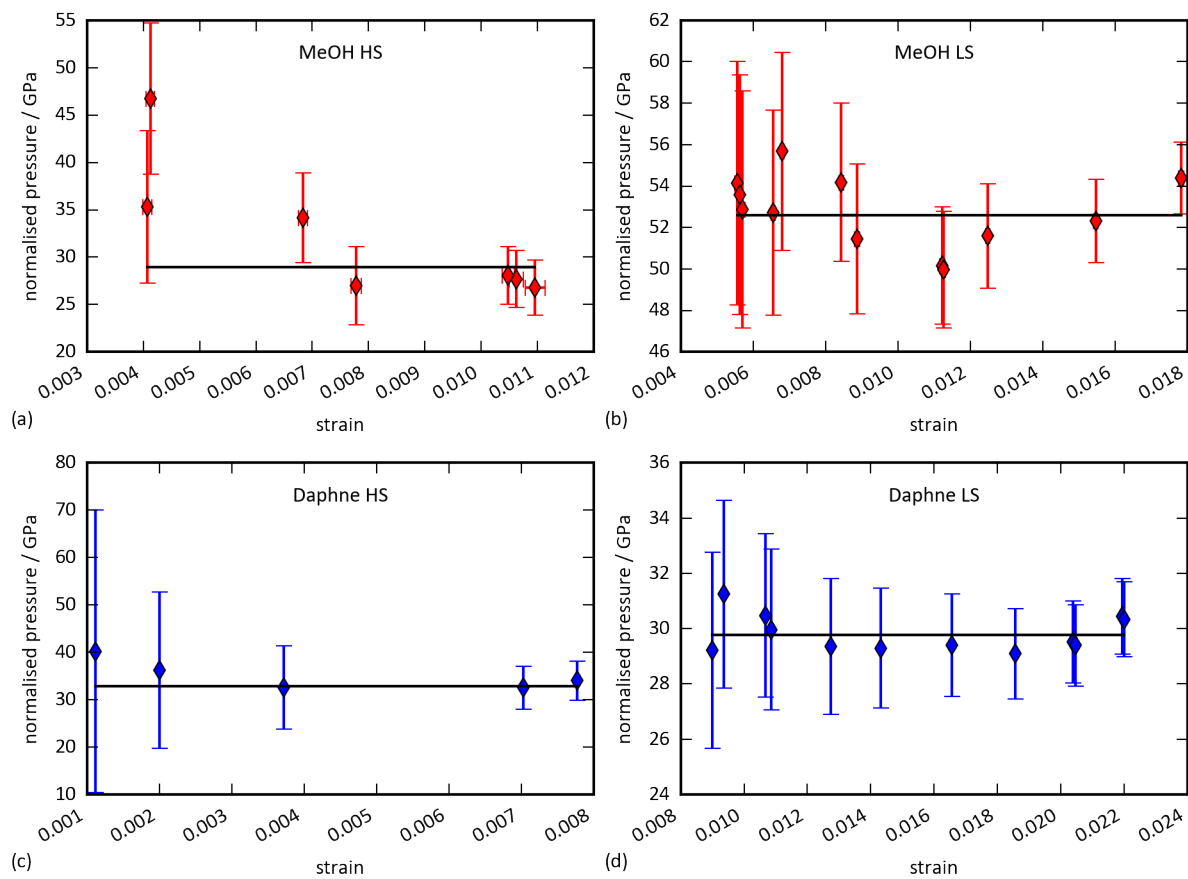


**Figure S7:** The normalised pressure vs. Eulerian strain from second-order Birch–Murnaghan fits for the (a) HS phase in MeOH, (b) LS phase in MeOH, (c) HS phase in Daphne oil, and (d) LS phase in Daphne oil.

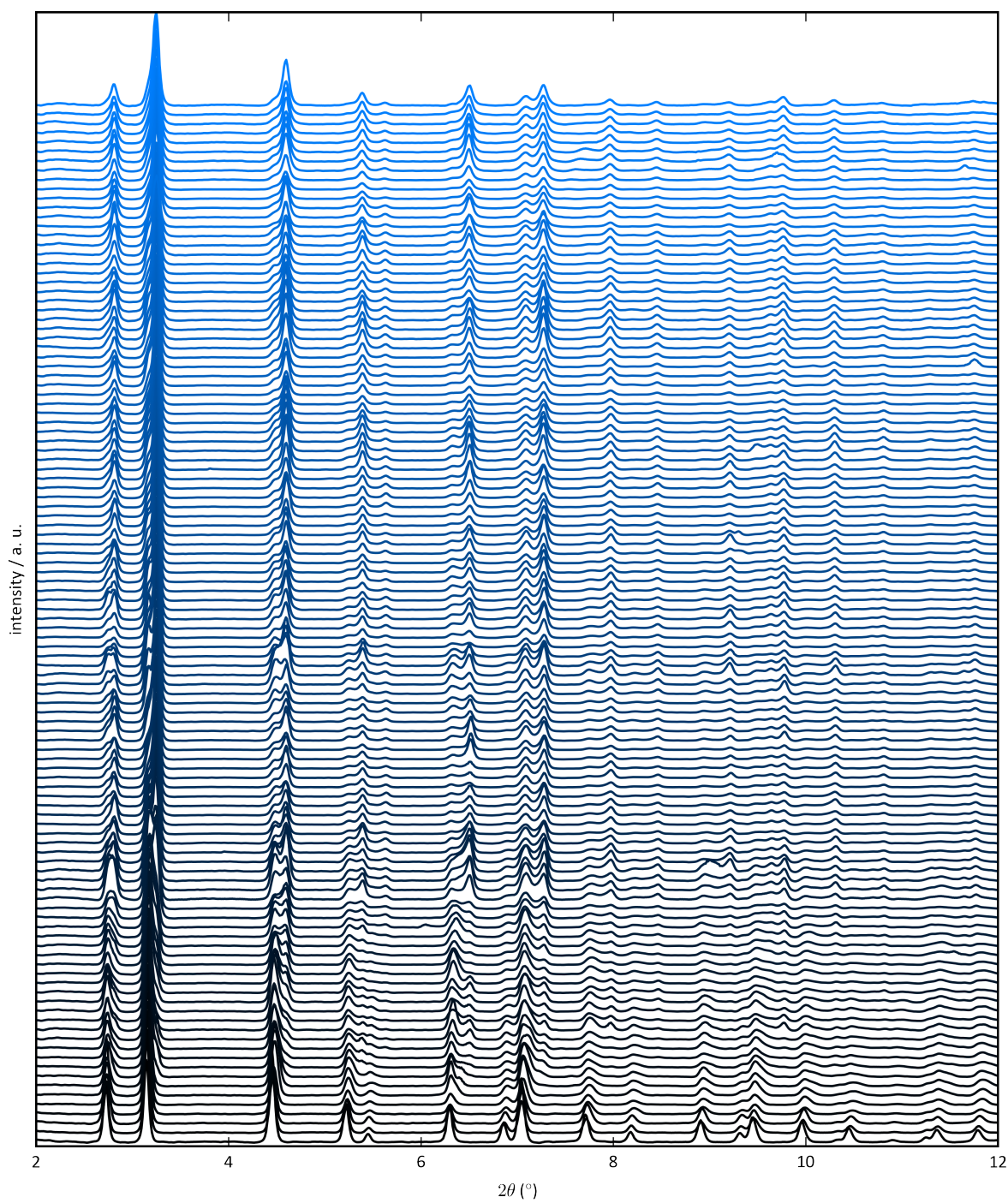


**Figure S8:** The XRD patterns of FePt(CN)<sub>6</sub> as a function of scan number (X-ray irradiation time) starting with scan 1 at the bottom (4 s exposure) up till scan 112 at the top (7.5 min exposure). All patterns were collected at 0.6 GPa with  $\lambda = 0.2897 \text{ \AA}$ .

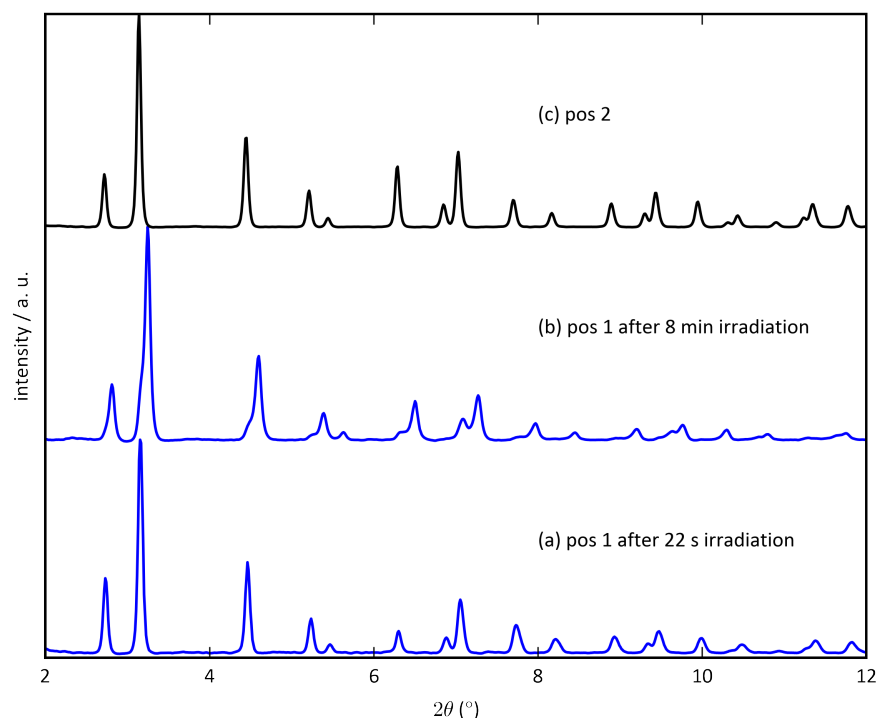


**Figure S9:** The XRD patterns of FePt(CN)<sub>6</sub> at (a) sample position 1 after 22 s of X-ray irradiation, (b) sample position 1 after 8 min of X-ray irradiation, and (c) the pristine sample (not previously X-ray irradiated) at position 2. All patterns were collected at 0.6 GPa with  $\lambda = 0.2897 \text{ \AA}$ .

## 4 Raman spectroscopy

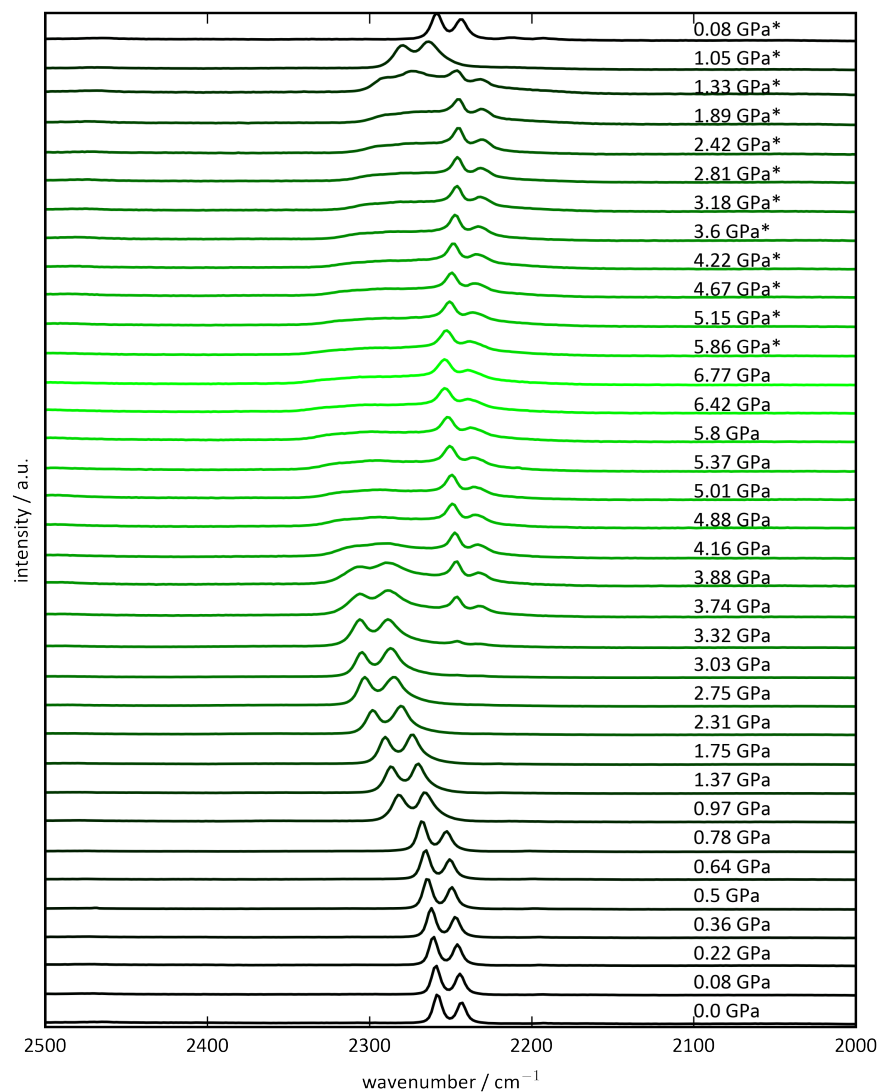


**Figure S10:** The high-wavenumber range of the Raman spectra of FePt(CN)<sub>6</sub> as a function of pressure. The data were collected on compression and spectra collected on decompression are denoted by an asterisk.

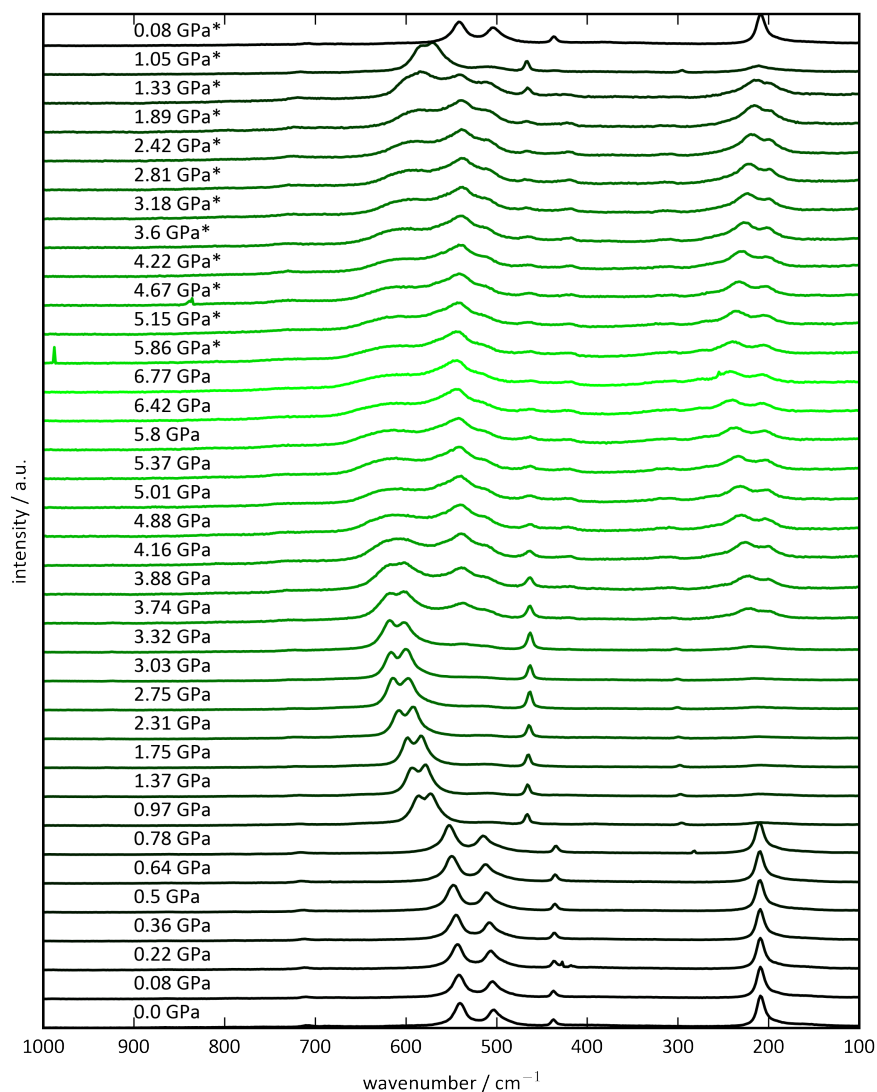


**Figure S11:** The low-wavenumber range of the Raman spectra of FePt(CN)<sub>6</sub> as a function of pressure. The data were collected on compression and spectra collected on decompression are denoted by an asterisk.

## 5 References

- (S1) C. Prescher and V. B. Prakapenka, *High Pressure Res.*, 2015, **35**, 223–230.  
 (S2) H. M. Rietveld, *Acta Crystallogr.*, 1967, **22**, 151–152.  
 (S3) A. A. Coelho, *J. Appl. Cryst.*, 2018, **51**, 210–218.

- (S4) G. S. Pawley, *J. Appl. Cryst.*, 1981, **14**, 357–361.
- (S5) F. Birch, *Phys. Rev.*, 1947, **71**, 809–824.
- (S6) F. D. Murnaghan, *Proc. Natl. Acad. Sci. U.S.A.*, 1944, **30**, 244–247.
- (S7) R. J. Angel, M. Alvaro and J. Gonzalez-Platas, *Z. Kristallogr.*, 2014, **229**, 405–419.
- (S8) A. Dewaele, M. Torrent, P. Loubeyre and M. Mezouar, *Phys. Rev. B*, 2008, **78**, 104102.
- (S9) J. M. Recio, J. M. Menéndez and A. O. de la Roza, *An Introduction to High-Pressure Science and Technology*, CRC Press, 2016.